



Atmospheric particulate-bound mercury (PBM₁₀) in a Southeast Asia megacity: Sources and health risk assessment

Ly Sy Phu Nguyen^{a,b,*}, To Thi Hien^{a,b}, Minh Tri Truong^{a,b}, Nguyen Doan Thien Chi^{a,b}, Guey-Rong Sheu^{c,d,**}

^a Faculty of Environment, University of Science, Ho Chi Minh City, Vietnam

^b Vietnam National University, Ho Chi Minh City, Vietnam

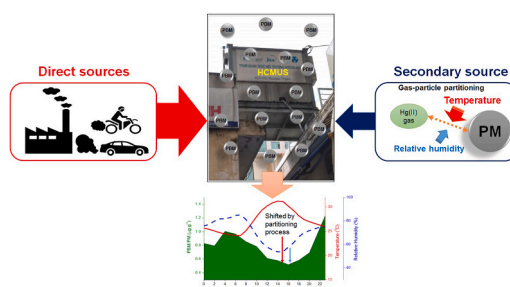
^c Department of Atmospheric Sciences, National Central University, Taoyuan, Taiwan

^d Center for Environmental Monitoring and Technology, National Central University, Taoyuan, Taiwan

HIGHLIGHTS

- First groundwork PBM study in Vietnam and Peninsula Southeast Asia (PSEA).
- PBM temporal variation and its driving mechanisms were explored.
- Both primary and secondary sources could contribute to PBM variations in HCMC.
- T is important driver of Hg content (PBM/PM) via gas-particle partitioning process.
- Set up foundation for upcoming studies and improve atmospheric Hg knowledge in PSEA.

GRAPHICAL ABSTRACT



ARTICLE INFO

Handling Editor: R Ebinghaus

Keywords:

Ho Chi Minh City
Southeast Asia
Particulate-bound mercury
Source apportionment
Health risk

ABSTRACT

Particulate-bound mercury (PBM) is a global environmental concern owing to its large dry deposition velocities and scavenging coefficients, both of which drive Hg into terrestrial and marine ecosystems. PBM observation studies have been widely conducted over East Asia, but comparable studies in Peninsular Southeast Asia (PSEA) remain scarce. This is the first study reporting PBM concentrations for Ho Chi Minh City (HCMC), the biggest metropolitan area in Vietnam. A total of 222 samples were collected in 2018 and contained an average PBM₁₀ (particulate matter – PM with diameter $\leq 10 \mu\text{m}$) concentration and Hg mass fraction (i.e. PBM/PM) of $67.3 \pm 45.9 \text{ pg m}^{-3}$ and $1.18 \pm 1.12 \mu\text{g g}^{-1}$, respectively. Although PBM concentration was lower than those reported in Chinese megacities, the Hg mass fraction was similar to those in China, suggesting strong enrichment from anthropogenic Hg emissions in HCMC. Traffic-induced particulate emission and deposition processes were major factors governing PBM temporal variation at our site. In addition, the prevailing southwest monsoon winds brought air masses that passed through industrial areas and were associated with a higher Hg mass fraction. Statistically significant positive correlations ($R^2 = 0.11\text{--}0.52$, $p < 0.01$) were observed for PBM with PM and the Hg mass fraction, indicating similar PM and Hg sources or oxidized Hg adsorption onto PM via gas-particle partitioning. Moreover, PCA results revealed a higher contribution of primary sources than secondary sources to PBM concentration variability in HCMC. A health risk assessment indicated that the PBM concentrations at

* Corresponding author. Faculty of Environment, University of Science, Ho Chi Minh City, Viet Nam.

** Corresponding author. Department of Atmospheric Sciences, National Central University, Taoyuan, Taiwan.

E-mail addresses: nlsphu@hcmus.edu.vn (L.S.P. Nguyen), grsheu@atm.ncu.edu.tw (G.-R. Sheu).

<https://doi.org/10.1016/j.chemosphere.2022.135707>

Received 14 April 2022; Received in revised form 4 July 2022; Accepted 11 July 2022

Available online 13 July 2022

0045-6535/© 2022 Elsevier Ltd. All rights reserved.

HCMC posed minimal non-carcinogenic risks ($HI < 1$) for children and adults, but dermal contact may act as an important exposure route since lightweight clothing is common among residents. This PBM dataset over PSEA, a region with high atmospheric Hg emissions, provides a valuable resource for the Hg scientific community to improve our understanding of Hg biogeochemical cycle.

1. Introduction

Mercury (Hg) is a toxic trace heavy metal of global concern because of its persistent and bio-accumulative features (Mason and Sheu, 2002; Driscoll et al., 2013). The majority of atmospheric Hg exists as gaseous elemental mercury (GEM), while minority components (i.e. $\leq 5\%$) are comprised of gaseous oxidized mercury (GOM) and particulate-bound mercury (PBM) (UNEP, 2013; Obrist et al., 2018; Nguyen et al., 2019a, 2019b). However, PBM is more sensitive to physicochemical processes, resulting in higher dry deposition velocities and scavenging coefficients when compared to GEM (Ariya et al., 2015). PBM deposition flux heavily depends on the emission type, either from local/regional sources or as a product of in-situ secondary formation (Mao et al., 2016; De Simone et al., 2017; Guo et al., 2020). In addition, mercury can magnify by bio-accumulation via food chain and inhalation (Beckers and Rinklebe, 2017). Therefore, newborns and toddlers are considered sensitive to PBM exposure (Andreoli and Sprovieri, 2017), which demands the need of PBM assessment despite its low atmospheric abundance.

Globally, PBM concentrations vary within the range from $< LOD$ to $\sim 400 \text{ pg m}^{-3}$ (Steffen et al., 2013; Zhang et al., 2019). In addition, Mao et al. (2016) pointed out a north-to-south decreasing gradient in ambient PBM concentration, which corresponds with a denser distribution of Hg sources in the Northern Hemisphere, especially in Asia. So far, observation studies mainly have focused on ambient PBM levels in mid-latitude regions, particularly suburban and background sites, while corresponding studies in tropical regions are still limited (Soerensen et al., 2010; Mao et al., 2016; Zhang et al., 2019). Industrial activities in Asian countries have released large Hg quantities (38.7% of the total anthropogenic Hg emissions to the air) into the atmosphere, mostly from anthropogenic and industrial sectors (UNEP, 2013; Wu et al., 2016). However, most atmospheric Hg monitoring studies in Asia are located in developed countries such as Taiwan, Japan, Korea, and China (Sakata and Marumoto, 2002; Kim et al., 2012; Nguyen et al., 2019a, 2022a; Sheu et al., 2010, 2019; Zhang et al., 2019), thus more studies from the SEA region are required to fill in the knowledge gap. Several model studies have estimated relatively high PBM concentrations over SEA (Amos et al., 2012; Weiss-Penzias et al., 2015; De Simone et al., 2017), which further highlights the need for PBM measurement data in the region to validate simulation results.

Both direct and indirect sources can exert an influence on atmospheric PBM concentrations (UN Environment, 2019; Guo et al., 2021; Nguyen et al., 2021a). Anthropogenic activity involving metal smelting, combustion and cement production are known PBM sources (UNEP, 2013; Wu et al., 2016), which can be identified using other aerosol components such as major ions and metals (Zhang et al., 2015a; Guo et al., 2017, 2021; Liu et al., 2019). Therefore, the transport pathway and atmospheric pollution origin can also be examined via the use of these ancillary data (Liu et al., 2019; Yu et al., 2019). On the other hand, gas-particle partitioning of oxidized Hg plays a key role in governing atmospheric PBM and GOM concentrations. Under favorable meteorological conditions, PBM formation could occur as GOM absorbs onto particulate matter (PM) via condensation and chemical reactions (Cheng et al., 2014; Sheu et al., 2019; Nguyen et al., 2021a). Greater GOM-to-PBM conversion has been found under lower temperatures, higher relative humidity, and higher PM concentrations, particularly that with higher carbonaceous content because it is considered a carrier of Hg (Rutter et al., 2007; Guo et al., 2021; Han et al., 2018; Nguyen et al., 2021a, 2021b).

Characterization of PBM temporal variations is important to understand the potential driving mechanisms, but is also dependent on site characteristics (Mao et al., 2016 and references therein). While PBM temporal variation is often unclear and inconsistent within the marine boundary layer (MBL) (Mao et al., 2012; Soerensen et al., 2010), frequent daytime PBM spikes from point sources or Hg-enriched areas are expected for urban areas (Choi et al., 2013; Sheu et al., 2019). Also, site elevation might exert an influence on the PBM diurnal pattern. For example, Mt. Lulin, Taiwan (2862 m a.s.l) has a PBM diurnal cycle regulated by vertical air mass movement that entrains Hg from the upper free tropospheric layer (Sheu et al., 2010). On the other hand, PBM temporal variation at a lower altitude site in Taiwan was more impacted by wind speed, wind direction and local emission sources (Sheu et al., 2019). The regional monsoon is also an important factor controlling PBM concentration variations due to its influence on transported air pollution pathways (Guo et al., 2020, 2021; Nguyen et al., 2021b). For instance, Guo et al. (2021) detailed the role of the Indian monsoon in governing the seasonal variation of PBM in Dhulikhel, Nepal, in which air masses transported from the Bay of Bengal during the monsoon season bring more rainfall and suppress PBM levels. Nonetheless, those aforementioned mechanisms are more common for mid-latitude regions while the monsoon impacts on PBM in tropical regions are poorly understood due to the lack of observation data (Mao et al., 2016; Zhang et al., 2019).

Vietnam is an active economic hub in the SEA region with an increasingly high population (ca. 100 million), especially in megacities like Hanoi and HCMC. The urbanization rate in Vietnam has accelerated significantly over the last two decades, which results in a higher level of air pollution. In particular, particle pollution poses a great health risk and has heightened the need to implement an effective environmental control strategy (Phung et al., 2016; Hien et al., 2019; Dat et al., 2021). Coal burning, artisanal gold mining and cement production are considered major Hg emission sources in Vietnam, with a total emission rate of 11.6 t yr^{-1} (UNEP, 2013). This figure is similar to Thailand (14.8 t yr^{-1}) while higher than neighboring countries in Peninsular SEA (PSEA) such as Cambodia (3.9 t yr^{-1}) and Laos (1.3 t yr^{-1}). Given PBM toxicity and its outsize effect to young population structure, attempts to characterize atmospheric Hg still requires a greater effort since observational studies in Vietnam and PSEA countries are scarce (UNEP, 2013; Zhang et al., 2019).

In this study, two intensive sampling IOPs were conducted at an urban site in HCMC, Vietnam to measure PBM_{10} and PM_{10} (hereby referred to as PBM and PM) in the dry and rainy seasons. PBM abundance, temporal variation and influencing factors were also investigated. Moreover, we interpreted the potential PBM sources in HCMC by adopting principal component analysis (PCA) using information from PM-bound metals and meteorological data. As HCMC is the most populous city in southern Vietnam, we further evaluated the PBM health risk via the use of a few indices. From our understanding, this is the first PBM observation study in Vietnam as well as in the PSEA region. Results from this study can help fill the global PBM data gap, provide a scientific basis for local and regional Hg emission control policies, assess PBM public health impacts and help to improve model simulations.

2. Site and methods

2.1. Site description

The sampling site was located on the rooftop of the Air Quality

Monitoring Station in University of Sciences campus, Ho Chi Minh City (HCMC, 10.7626°N, 10.6819°E, Fig. 1). This site is situated near Nguyen Van Cu Street, which is heavily congested with traffic activity during rush hours (Hien et al., 2019; Nguyen et al., 2022b). HCMC is an economic hub and a highly urbanized city within the PSEA region. In addition, industrial areas within a 60-km radius of the sampling site and with a variety of production types and scales are potential local Hg emission sources (Fig. S1).

Vietnam is located along the east coast of the Indochina Peninsula with a typical tropical climate. Its weather pattern is mainly governed by the East Asia monsoon system, with the northeast monsoon dominating during December–April while the southwest monsoon prevails between May and September, leaving the other months as the transitional period (Wu, 2017; Le et al., 2019). Ambient temperature is normally higher along the central coastal region, while a greater seasonal temperature gap is found in northern regions as compared to southern regions (Le et al., 2019). In 2018, an average temperature of 28.8 °C and a total of 2440 mm rainfall were recorded for HCMC, characterizing a hot and humid tropical climate in the study area.

2.2. PM₁₀ sampling and Hg analysis

In this study, PM sampling was carried out every 2 h (i.e. 1:00, 3:00, 5:00, etc ...) using a portable high-volume air sampler (Sibata, Japan) at 500 L min⁻¹ in two intensive IOPs in 2018 (IOP1: Jan 20 – Feb 13 i.e. dry season and IOP2: July 8–26 i.e. rainy season). A PM impactor was also deployed to achieve a cut size of 10 μm. Sampling flow rate was calibrated every 48 h to ensure an accurate sampling volume was recorded. Our short sampling time strategy allowed us to observe the PBM diurnal pattern. Glass-fiber filters (∅ = 110 mm, Advantec, Japan) used for sampling were pre-baked at 450 °C (8 h) to remove possible residual Hg. The Hg amount in filter blanks was lower than 0.07 ng, ensuring minimal contamination. After sampling, filters were kept at -20 °C before being shipped to National Central University in Taiwan for total Hg analysis. PM mass concentration was determined by gravimetric method, using a microbalance with 1.0 μg readability. Filters were weighed before and after sampling at specific equilibration conditions (25 ± 2 °C T and 35 ± 5% RH). Further details related to sampling and PM mass concentration determination can be found in Hien et al. (2019).

Total Hg amount in one-fourth of each filter was quantified by the MA3-Solo thermal decomposition Hg analyzer (NIC, Japan) following USEPA Method 7473. This method has been widely applied for Hg analyses using thermal decomposition (McLagan et al., 2016, 2019; Zheng et al., 2021a), thus was applicable for the PM samples. The dual-stage

temperature program consists of an initial step at 350 °C (180 s), followed by a heat ramp to 850 °C (360 s). Water vapor and VOCs are eliminated during the first step, leaving the zero-air stream (at 0.2 L min⁻¹) carrying the converted Hg in the second step onto a gold-coated silica trap. GEM is then released from the trap at 600 °C (30 s) and quantified by atomic absorption spectrometry (AAS) at 253.7 nm. Hg masses at 0.5, 1.0, 5.0, 10, 50, 100, and 150 ng Hg were used for constructing the calibration curve, which achieved linearity of R² = 0.9999. The average blank value (0.067 ng) was subtracted from all sample Hg mass determinations prior to calculating the ambient concentration. Hg mass fraction (μg g⁻¹) and PBM ambient concentration (pg m⁻³) was then calculated by dividing the analyzed Hg mass over the equilibrated PM₁₀ mass and sample volume, respectively.

QA/QC parameters for the analysis were applied based on USEPA Method 7473. Method blanks and liquid standard recovery checks were periodically performed, with < MDL (0.05 ng ca. 1 pg m⁻³) Hg mass and recovery rates of 98.8 ± 2.7% (n = 31), respectively. Method precision was verified by NIST SRM 1648a (urban particulate matter) and SRM 2685c (bituminous coal), with recovery rates of 99.8 ± 7.2% (n = 5) and 95.7 ± 3.0% (n = 6), respectively. Hg carry-over effect was also evaluated by heating samples with high Hg masses twice, and the residual Hg amount was always lower than 0.2% of the first run. These results demonstrated good analytical precision and accuracy of the Hg determination method used in this study.

2.3. Measurement of metals and meteorological parameters

In addition to Hg, we also carried out heavy metals analysis (Al, Mn, Cu, Cr, Pb, Ni, As and Sr) using inductively coupled plasma mass spectrometry (ICP-MS; model 7700x, Agilent, USA) following the US EPA method 6020B and Method 200.8 Rev 5.4. Samples were thoroughly mixed into a solution of HNO₃:HCl = 1:2 (v/v), then digested at 180 °C for 45 min and subsequently cooled at 50 °C. The leachate was then filtered through a 0.45-μm PTFE syringe into a 50-mL polypropylene centrifuge tube, and stored until analysis. SRM 1648a was tested for method accuracy and yielded recovery rates within 85–115% for selected metals. More information on the QA/QC parameters can be found in Truong et al. (2022). Besides, meteorological parameters including temperature (T), relative humidity (RH), wind speed (WS), and rainfall depth were obtained from a nearby weather station (ca. ~4 km away, Fig. 1).

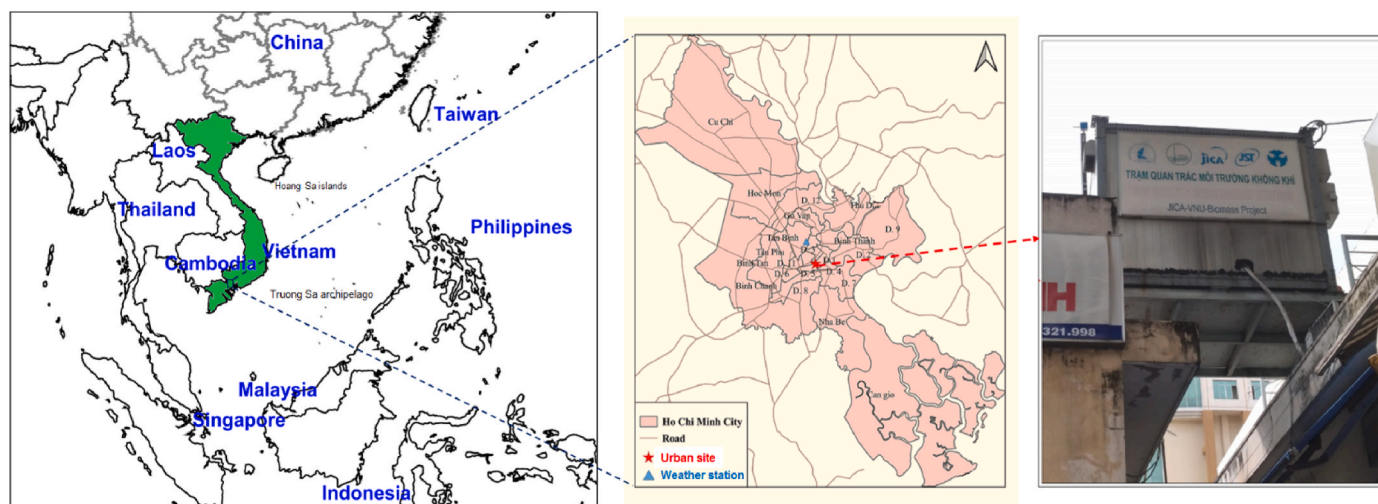


Fig. 1. Location of the sampling site and air monitoring and weather stations; with the PM sampler located on the rooftop of the station.

2.4. Backward trajectory (BWT) calculation and cluster analysis

BWT analysis was performed to investigate the origin and transport pathway of air parcels arriving at HCMC, using the Hybrid Single Particle Lagrangian Integrated Trajectory (HYSPLIT) model (Draxler and Rolph, 2010) with meteorological input from NCEP Global Data Assimilation System database (GDAS-1, $1^\circ \times 1^\circ$ resolution). In this study, 120-h BWTs were calculated every 2 h at 200 m a.g.l. (i.e. within the PBL height) corresponding to each sampling time. A cluster analysis was performed with TrajStat software (Wang et al., 2009) to classify air masses sharing similar trajectory patterns.

2.5. Planetary boundary height (PBL) height

To determine the impact of the PBL on the PBM diurnal variation, PBL height data was obtained from the Modern-Era Retrospective analysis for Research and Applications, Version 2 (MERRA-2). MERRA-2 was assimilated by the modern hyperspectral radiance and microwave observation, alongside GPS-Radio Occultation datasets. The key components of MERRA-2 are the GEOS atmospheric model and the GSI analysis scheme which uses a cubed-sphere horizontal discretization. MERRA-2 has a spatiotemporal resolution of $0.5^\circ \times 0.625^\circ$ and 6 h. The PBL data was taken from MERRA-2 reanalysis product M2T1NXFLX (MERRA-2 tavg1_2d_flux_Nx). More details regarding MERRA-2 reanalysis can be found in Buchard et al. (2017).

2.6. Inhalation exposure and health risk assessment

Since Hg poses an insignificant carcinogenic effect (USEPA, 2017), PBM potential non-carcinogenic effect was evaluated instead via hazard quotient (HQ) and hazard index (HI) in this study. Human health can be greatly impacted if exposed to Hg via non-dietary ingestion, inhalation or dermal contact pathways (WHO, 2000). Therefore, the average daily PBM intake ($\text{mg kg}^{-1} \text{day}^{-1}$) via each pathway was calculated using the following equations:

$$\text{ADD}_{\text{ing}} = \frac{\text{IR}_{\text{inh}} \times [\text{PBM}] \times \text{EF} \times \text{ED} \times \text{CF}}{\text{BW} \times \text{AT}} \quad (1)$$

$$\text{ADD}_{\text{inh}} = \frac{\text{IR}_{\text{inh}} \times [\text{PBM}] \times \text{EF} \times \text{ED} \times \text{CF}}{\text{BW} \times \text{AT}} \quad (2)$$

$$\text{ADD}_{\text{derm}} = \frac{[\text{PBM}] \times \text{EF} \times \text{ED} \times \text{SA} \times \text{AF} \times \text{ABS} \times \text{CF}}{\text{BW} \times \text{AT}} \quad (3)$$

where [PBM] is the ambient PBM concentration (ng m^{-3}), EF the exposure frequency (days yr^{-1}), ED the exposure duration (years), BW the body weight (kg), AT the average exposure time (days) and CF a conversion factor ($10^{-6} \text{kg mg}^{-1}$). Specific parameters for each exposure pathway were also evaluated such as ingestion rate (IR_{ing} , mg day^{-1}), inhalation rate (IR_{inh} , $\text{m}^3 \text{day}^{-1}$), dermal surface exposure area (SA, cm^2), adherence factor (AF, $\text{mg cm}^{-2} \text{day}^{-1}$), and dermal absorption factor (ABF), with values shown in Table S3. Given the young population structure of HCMC with around 25% of children under 14 years old, both children and adults were evaluated for PBM health risk, using the equations below:

$$\text{HQ}_i = \frac{\text{ADD}_i}{\text{RfD}_i} \quad (4)$$

$$\text{HI} = \sum \text{HQ}_i = \text{HQ}_{\text{ing}} + \text{HQ}_{\text{inh}} + \text{HQ}_{\text{derm}} \quad (5)$$

where RfD ($\text{mg kg}^{-1} \text{day}^{-1}$) is the reference dose of PBM via ingestion (1.6×10^{-4}), inhalation (3.0×10^{-4}) and dermal (2.1×10^{-5}) pathways (USEPA, 2017; Cui et al., 2020). An HI < 1 value indicates a non-adverse health effect by PBM via an exposure pathway while an HI ≥ 1 indicates a high probability of PBM health risk among the chosen age group in the

study area.

3. Results and discussion

3.1. General characteristics of PBM₁₀ concentrations

A total of 222 samples were collected: 119 samples in the dry season and 103 samples in the rainy season. A summary of the PM and PBM concentrations during the study period are presented in Table 1. In our study, the PM concentration ranged from 5.0 to 210.6 $\mu\text{g m}^{-3}$ with an average of $76.7 \pm 46.8 \mu\text{g m}^{-3}$ while PBM concentrations fluctuated widely from 14.6 to 306.6 pg m^{-3} with an average of $67.3 \pm 45.9 \text{pg m}^{-3}$. From Hien et al. (2019), PM_{2.5} concentrations at HCMC are on average $39.1 \pm 14.9 \mu\text{g m}^{-3}$, suggesting a PM coarse fraction (i.e. PM_{10-2.5}) of nearly 50%.

Table 2 shows an average (\pm S.D.) PBM concentration in HCMC of $67.3 \pm 45.9 \text{pg m}^{-3}$, comparable to urban sites in Poland (Siudek et al., 2016; Pyta and Rogula-Kozłowska, 2016) and Tokyo, Japan (Sakata and Marumoto, 2002). In addition, this value is 4 times higher than in Taoyuan, Taiwan (Sheu et al., 2019) and sites in Canada (Poissant et al., 2005; Song et al., 2009), about 8 times higher than in Beltsville, USA (Ren et al., 2016) and 12 times higher than in Seoul, Korea (Kim et al., 2012). However, the PBM level at HCMC was significantly lower than urban sites in China like Beijing (3.2–8.5 times, Schleicher et al., 2016; Huang et al., 2020), Shanghai (4.7–5.7 times, Xiu et al., 2005; Han et al., 2018), Nanjing (16.3 times, Zhu et al., 2014), and Qingdao (2.8–4.3 times, Zhang et al., 2015b) as well as sites in Kathmandu Valley (12.6 times, Guo et al., 2017), and Dhulikhel, Nepal (1.6 times, Guo et al., 2021). Local anthropogenic influences including industrial activities, heavy coal/fuel combustion and winter heating can explain the elevated PBM concentrations at urban sites in China and basin areas down the southern slope of the Himalayas (Fu et al., 2015; Liu et al., 2019; Guo et al., 2017, 2021). In general, as a tropical climate city with medium-scale urbanization and a industrialization level with no winter heating demand, a comparatively moderate PBM pollution level was observed at HCMC as compared with other studies worldwide. Moreover, apart from measurement data, model simulations also help to estimate PBM concentration metrics on a global scale. By integrating a biomass burning inventory into the ECHMERIT model, De Simone et al. (2017) achieved a better model-observation agreement for PBM measured at ground-based sites, and estimated an annual PBM concentration of 6.5–10 pg m^{-3} for areas around HCMC. Accordingly, the high PBM value we obtained (67.3pg m^{-3}) was not well-captured by that model, possibly due to the higher contribution from anthropogenic activities. Therefore, our results also suggested that a timely update of mercury emission inventory data in PSEA, particularly for megacities, is needed to improve the accuracy of model simulations.

Furthermore, the use of the Hg mass fraction (i.e. PBM/PM ratio)

Table 1
Summary of PM₁₀, PBM₁₀ and Hg mass fraction during the study period.

		PM ₁₀ ($\mu\text{g m}^{-3}$)	PBM ₁₀ (pg m^{-3})	PBM ₁₀ /PM ₁₀ ($\mu\text{g g}^{-1}$)
Total	Mean \pm S.D.	76.7 ± 46.8	67.3 ± 45.9	1.18 ± 1.12
n = 222	Min - Max	5.0–210.6	14.6–306.6	0.33–11.61
Dry	Mean \pm S.D.	110.8 ± 36.1	85.1 ± 53.7	0.78 ± 0.46
n = 119	Min - Max	47.7–210.6	29.7–306.6	0.33–3.60
Wet	Mean \pm S.D.	37.4 ± 18.0	46.7 ± 20.5	1.64 ± 1.44
n = 103	Min - Max	5.0–79.7	14.6–156.8	0.44–11.61

Table 2

Summary of PBM concentrations and the Hg mass fraction in this study and various sites worldwide.

Sampling sites	Size	Hg Conc. (pg m ⁻³)	PBM/PM(μg g ⁻¹)	References
Ho Chi Minh City	PM ₁₀	67.3 ± 45.9	1.18 ± 1.12	This study
Beijing, China	TSP	220 ± 130	0.8 ± 0.3	Huang et al. (2020)
Beijing, China	TSP	573 ± 551	1.40 ± 0.92	Schleicher et al. (2016)
Beijing, China	PM _{2.5}	Day: 263 ± 246; Night: 280 ± 383	–	Schleicher et al. (2016)
Shanghai, China	TSP	318 ± 144	–	Han et al. (2018)
Shanghai, China	TSP	233–529	1.05–2.85	Xiu et al. (2005)
Xi'an, China	TSP	640 ± 540	–	Xu et al. (2015)
Nanjing, China	PM ₁₀	1100 ± 570	–	Zhu et al. (2014)
Qingdao, China	TSP	Dust: 290; Non-dust: 190	Dust: 0.69; Non-dust: 1.10	Zhang et al. (2015b)
Kathmandu Valley, Nepal	TSP	850.5 ± 926.8	2.59 ± 2.07	Guo et al. (2017)
Dhulikhel, Nepal	TSP	108.7 ± 86.2	0.42 ± 0.24	Guo et al. (2021)
NCU, Taiwan	PM _{2.5} *	18.7 ± 86.8	–	Sheu et al. (2019)
Seoul, Korea	TSP	6.8 ± 6.5	0.18	Kim et al. (2012)
Tokyo, Japan	PM ₁₀	98 ± 51	–	Sakata and Marumoto (2002)
Okinawa, Japan	PM _{2.5}	3.0 ± 2.4	0.20	Chand et al., (2008)
Detroit, USA	TSP	94	–	Keeler et al. (1995)
Beltsville, Maryland, USA	PM _{2.5} *	8.6 ± 56.8	–	Ren et al. (2016)
Toronto, Canada	PM _{2.5} *	21.5 ± 16.4	–	Song et al. (2009)
St. Anicet, Canada	PM _{2.5} *	26 ± 54	–	Poissant et al. (2005)
Poznan, Poland	TSP	40 ± 50	–	Siudek et al. (2016)
Zabrze, Poland	PM ₁₀	63.6 ± 53.0	–	Pytaand Rogula-Kozłowska, 2016
Terra Nova Bay, Antarctica	PM ₁₀	87 ± 8	–	Illuminati et al. (2020)

Data with (*) indicates Tekran® 1135 measurements.

could be useful in assessing the evidence of Hg enrichment and its related sources, particularly for sites where PBM is associated with both natural and anthropogenic origins (Schleicher et al., 2016; Guo et al., 2020, 2021). At HCMC, the mean (±S.D.) Hg mass fraction was 1.18 ± 1.12 μg g⁻¹, ranging from 0.33 to 11.61 μg g⁻¹. This value is significantly higher than street dust samples collected in HCMC (0.12 ± 0.19 μg g⁻¹), and greater than Hg mass fraction values reported for local raw coal for thermal power plants in Vietnam (0.06–0.14 μg g⁻¹; Hien et al., 2018) or natural dust in China (0.06–0.3 μg g⁻¹; Schleicher et al., 2016). The comparison results suggested there was Hg enrichment on atmospheric particles at our sampling site, a process favored by both accumulation from ambient air and input from anthropogenic sources (Han et al., 2018; Guo et al., 2017, 2021; Nguyen et al., 2021a). Although the Hg mass fraction was only evaluated for PM₁₀ in our study, some studies have revealed greater Hg accumulation in finer PM fractions (e.g. PM_{2.5}; Zhu et al., 2014; Chen et al., 2016; Tang et al., 2019). Therefore, it is possible that higher Hg mass fractions could be found in smaller particle sizes (i.e. PM_{2.5}) at HCMC and could be a target for our upcoming studies.

Table 2 shows that the Hg mass fraction in HCMC is comparable to

densely-populated areas in China such as Beijing (1.40 μg g⁻¹), Qingdao (1.10 μg g⁻¹), and Shanghai (1.05–2.85 μg g⁻¹) while lower than in Kathmandu Valley, Nepal (2.59 μg g⁻¹). On the other hand, our ratio was significantly greater than in Seoul, Korea (0.18 μg g⁻¹), Okinawa, Japan (PBM_{2.5}/PM₁; 0.20 μg g⁻¹) and Dhulikhel, Nepal (0.42 μg g⁻¹). In studies from China, local anthropogenic sources (e.g., coal combustion, cement productions, and metal smelting) have been found responsible for elevated ambient PBM levels that drove up PBM/PM ratios (Wu et al., 2016, 2017; UN Environment, 2019). Also, low-grade coal and fuel quality could have a substantial effect on aerosol Hg concentrations, which have led to a higher Hg mass fraction in Nepal (Huang et al., 2016; Guo et al., 2021). These comparisons further imply the role of anthropogenic sources and industrial sectors in increasing Hg loadings on particles in urban areas, with HCMC being a typical example. Owing to the relatively high PBM/PM ratio, the impact of anthropogenic and industrial sources on PBM pollution should be carefully evaluated for HCMC. Stricter air pollution assessment and regulation should be imposed to avoid further increasing the ambient PM and PBM concentrations in residential areas.

In addition, a significant positive PBM-PM correlation ($p < 0.01$) was observed with a better correlation in the dry season ($R^2 = 0.31, p < 0.01$, Fig. 2A) than in the rainy season ($R^2 = 0.13, p < 0.01$, Fig. 2B). These positive correlations suggested PBM increases resulted from PM mass

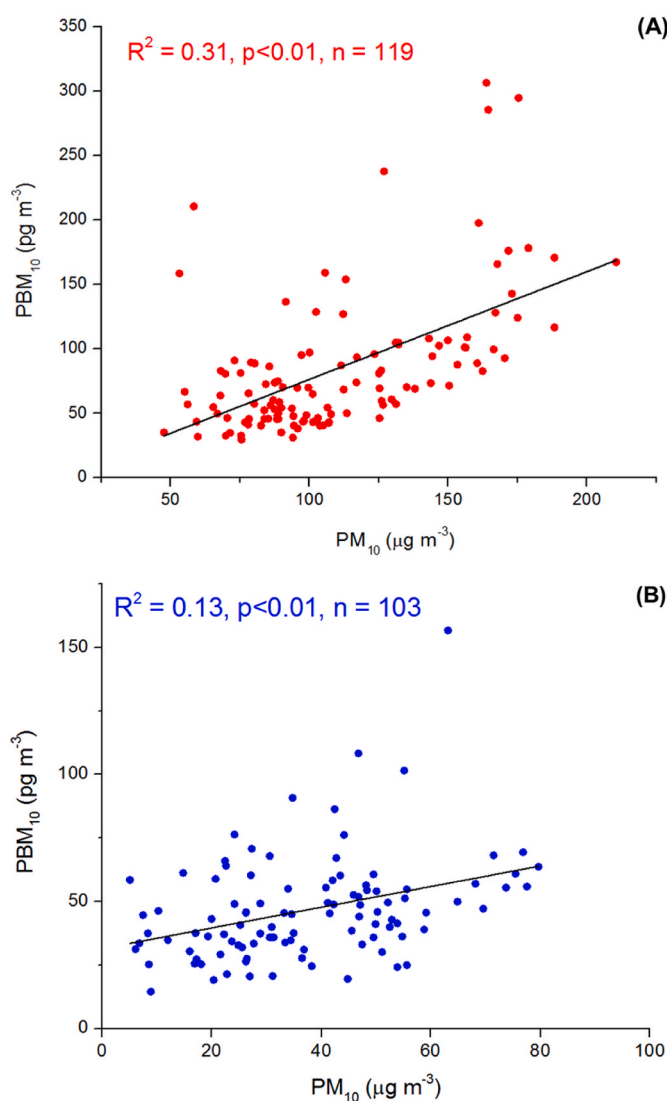


Fig. 2. Correlation between PM₁₀ and PBM₁₀ during the (A) dry season and (B) rainy season.

increases at our site. However, PBM-PM correlations were comparatively low in both seasons and lower than those of an urban site in China ($R^2 = 0.67$, Zhu et al., 2014) which implies the possible contribution of other indirect processes on the PBM concentration. Similarly, significant positive correlations were also observed between PBM and the PBM/PM ratio in both the dry season ($R^2 = 0.52$, $p < 0.01$, Fig. 3A) and the rainy season ($R^2 = 0.11$, $p < 0.01$, Fig. 3B). This suggests either there were similar sources for PBM and PM or oxidized Hg adsorption onto PM via gas-particle partitioning was significant (Huang et al., 2016; Guo et al., 2017; Han et al., 2018). However, these correlations were comparatively lower than the city of Kanpur, India ($R^2 = 0.77$, $p < 0.01$, Guo et al., 2020) in which direct Hg sources such as anthropogenic emission, fuel combustion and crop burning dominate. Similar positive PBM-PM correlations to our study were observed in Kathmandu Valley and Dhulikhel, Nepal (Huang et al., 2016; Guo et al., 2017, 2021), indicating either similar origins or overlapping atmospheric processes between the two species in both sites. It should be noted that atmospheric PBM sources include direct emission sources and indirect influences from atmospheric processes, which involve PM as an adsorption surface for GOM locally or along the transport pathway (Guo et al., 2017; Huang et al., 2020; Nguyen et al., 2021a). Therefore, the addition of a more complex variety of sources or atmospheric processes during the rainy

season might weaken the PBM-PM relationship as compared to the dry season (Zhang et al., 2015b; Tang et al., 2019; Nguyen et al., 2021a). This has been demonstrated by studies in Beijing, China and Mt. Lulin, Taiwan where weak PBM-PM correlations were attributed to contributions from numerous atmospheric sources and processes of PBM (Tang et al., 2019; Nguyen et al., 2021a). Overall, the correlation analysis suggested anthropogenic activities and gas-particle transformation as important contributors to PBM characteristics in HCMC, while more details are discussed in the following sections.

3.2. Temporal variation and driving factors

Despite a two-month sampling window, our sampling strategy has enabled us to examine both seasonal and diurnal variations of PBM and PM (Table 1 and Fig. 4). Regarding the seasonal variation, PM concentrations fluctuated between 47.7 and 210.6 $\mu\text{g m}^{-3}$ with a mean of $110.8 \pm 36.1 \mu\text{g m}^{-3}$ in the dry season, while a narrower range (5.0–79.7 $\mu\text{g m}^{-3}$) and lower mean value ($37.4 \pm 18.0 \mu\text{g m}^{-3}$) were found in the rainy season. Similarly, PBM concentrations varied between 29.7 and 306.6 pg m^{-3} ($85.1 \pm 53.7 \text{pg m}^{-3}$) in the dry season compared to the range of 14.6–156.8 pg m^{-3} ($46.7 \pm 20.5 \text{pg m}^{-3}$) in the rainy season. Mann-Whitney U tests indicated significant seasonal variations for both species ($p < 0.01$), showing 2.9 times and 1.8 times higher mean values in the dry season than the rainy season. Several factors can affect PBM temporal variation, most of which include air mass origins and transport paths, atmospheric processes, and meteorological factors (Sprovieri et al., 2010; Mao et al., 2016; Nguyen et al., 2019b; Sheu et al., 2019). At HCMC, the distinct PBM seasonal variation could be controlled by the difference in deposition processes between the two seasons. Scavenging by rainfall (i.e. wet deposition) commonly suppresses ambient PBM levels via the washout effect, with rainfall depth playing the predominant role in driving Hg wet deposition (Sheu and Lin, 2013; Ariya et al., 2015; Fu et al., 2016; Nguyen and Sheu, 2019). During the sampling period, higher rainfall (Fig. S2A) and lower PBM concentrations (37.4%) were observed in the rainy season as compared to the dry season (Table 1), suggesting rainfall amount as a major factor that controls PBM seasonal cycle at HCMC.

On the other hand, wind speed plays the dominant role in governing PM dry deposition velocity and PBM dry deposition (Zhang et al., 2015a, b; Nguyen et al., 2019b) as higher wind speed facilitates greater dry deposition, which reduces both PM and PBM concentrations. For instance, Nguyen et al. (2019b) linked lower wind speeds in summer to lower PBM dry deposition when compared to winter months at Mt. Lulin, Taiwan. In our study, a higher wind speed was observed in the rainy season (Fig. S2B), suggesting greater PBM dry deposition as compared to the dry season. In addition, atmospheric accumulation might contribute to PBM seasonal variation, in which PBL height plays a key factor (Xu et al., 2015; Hien et al., 2019). A study in East China showed a weak negative correlation between PBM and PBL height, suggesting the impact of weak diffusion on observed elevated PBM concentrations (Qin et al., 2019). During the study period, the mean PBL height was around 2 times lower in the rainy season (465 m, Fig. S2C) than in the dry season (895 m, Fig. S2C), suggesting a possible greater PBM accumulation in the rainy season. However, as the ambient PBM level was lower in the rainy season (Table 1), deposition processes tended to dominate over this period and outweighed the accumulation effect in controlling the PBM and PM seasonal variation. Overall, the seasonal discrepancy in PBM concentrations in HCMC was mainly governed by deposition processes, in which higher deposition in the rainy season attenuated PBM levels.

In contrast to PBM concentrations, a reversed seasonal pattern (dry < rainy) was observed for the Hg mass fraction, with mean values (\pm S. D.) of $0.78 \pm 0.46 \mu\text{g g}^{-1}$ and $1.64 \pm 1.44 \mu\text{g g}^{-1}$, respectively (Table 1). Fig. 5 shows the backward trajectories arriving at HCMC during the two IOPs, with air masses passing the Binh Duong and Dong Nai industrial zones from the N-NE direction in the dry season and the Long An

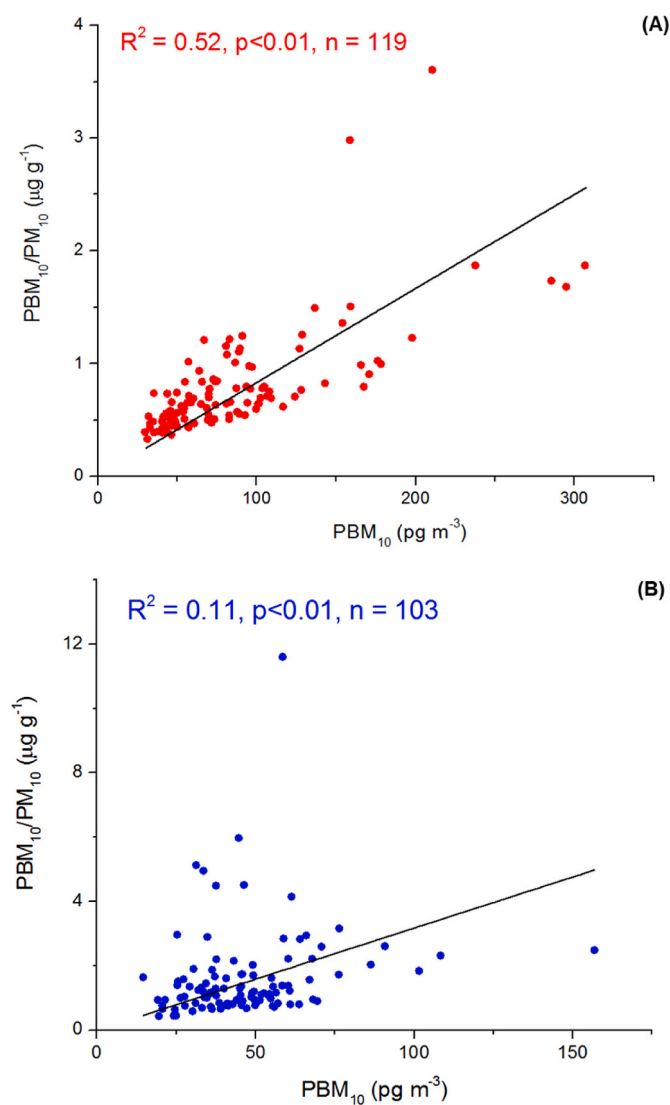


Fig. 3. Relationship between PBM and PBM/PM during the (A) dry season and (B) rainy season.

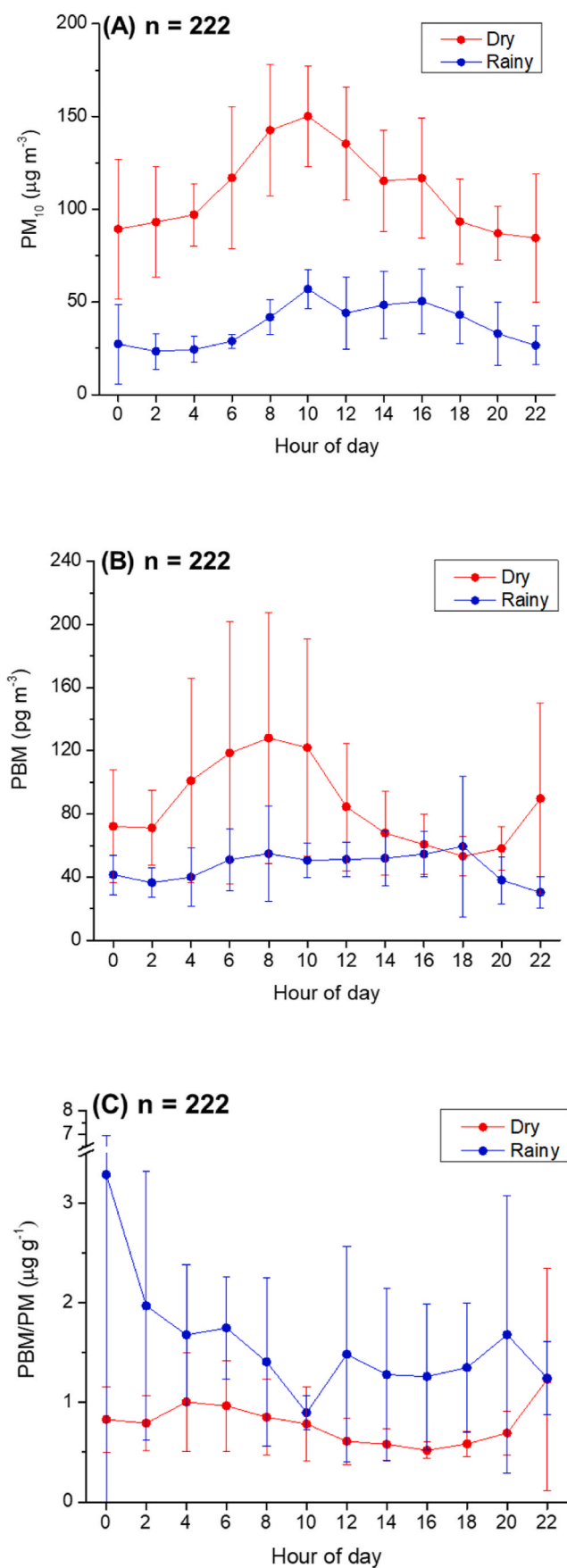


Fig. 4. Diurnal variation of (A) PM_{10} ; (B) PBM_{10} and the (C) PBM/PM ratio in the dry and rainy seasons at HCMC.

industrial zone from the W-SW direction in the rainy season (Fig. S1). This air mass pattern was governed by monsoonal shifts, with a prevailing northeast and southwest monsoon during the dry and rainy season, respectively (Nguyen et al., 2022b). Fig. S1 describes the complex cluster of industrial zones (i.e. industrial clusters in different regions often have different characteristics) within a 20–50 km radius near the sampling site. Potential Hg emissions sources like small-scale metallurgy, cement production, and manual steel-iron reproduction are typical in the W-SW sector while lighter industries including electroplating, manufacturing and textile industries are prominent in the N-NE sector. Thus, the discrepancy in types and scales of industrial morphologies could contribute to the difference in Hg emissions and the Hg mass fraction (Driscoll et al., 2013; Ariya et al., 2015). For instance, metal smelting and cement production tend to emit excessively large GEM and/or GOM quantities (Wu et al., 2016, 2017), which could contribute to an elevated Hg mass fraction. Prominent cement production activity in the Long An industrial zone (Fig. S1) might contribute as a significant PBM source, and lead to a higher Hg mass fraction in the rainy season (Table 1).

Regarding the diurnal variation, a clear PM unimodal distribution was observed but less pronounced in the rainy season (Fig. 4A). More frequent and higher rainfall amount (Fig. S2A) in the rainy season (79% days with rain) as compared to the dry season (20% days with rain) may have suppressed ambient PM levels. A PM peak was observed during rush hour (i.e. 8–9 am) and subsequently decreased in both seasons (Fig. 4A–B) as a result of increased turbulence and reduced vehicular emission. A rush-hour peak was also reported for $PM_{2.5}$ diurnal variation in a previous HCMC study (Hien et al., 2019), and was attributed to vehicle exhaust and anthropogenic activities within the region. Similar diurnal patterns were found for PBM in both seasons (Fig. 4B), with a more explicit rush hour peak in the dry season compared to the rainy season. As a consequence, PM mass concentration increase with traffic congestion acts as a precursor for more oxidized Hg partitioning and drove the PBM diurnal pattern (Cheng et al., 2014; Nguyen et al., 2021a). Previous studies have suggested that a lower PBL height may facilitate Hg re-distribution and accumulation onto particles leading to a higher PBM concentration (Gratz et al., 2013; Xu et al., 2015). However, despite a low PBL height from nighttime until early morning in both seasons (Fig. S3A), PBM concentrations during these hours remained low. This is different from other studies in Xiamen, China (Xu et al., 2015), Lake Michigan, USA (Gratz et al., 2013) and Shanghai, China (Qin et al., 2019) where atmospheric dispersion drove PBM diurnal cycles. For our site, as PBM and PM peaks both occurred during rush hour, effects from local emissions may have outweighed PBL modulation in controlling their diurnal patterns.

In contrast to PBM, higher (t -test, $p < 0.05$) nighttime (7 a.m.–6 p.m.) Hg mass fraction was observed as compared to daytime (6 p.m.–7 a.m.) in both seasons (Fig. 4C), suggesting the dependence of the Hg mass fraction diurnal variation on secondary formation processes (Guo et al., 2017, 2020; Nguyen et al., 2021a). While the type and scale of local anthropogenic sources can influence Hg mass fraction seasonality, indirect secondary sources (i.e. gas-particle partitioning) can further alter the Hg mass fraction diurnal variation. T and RH serve as major driving factors for gas-particle partitioning of oxidized Hg (Rutter et al., 2007; Kim et al., 2012; Choi et al., 2013). Hg mass fraction showed negative correlations with T ($p < 0.01$, Figs. S4A–B) and positive correlations with RH ($p < 0.01$, Figs. S5A–B) in both seasons, suggesting contribution from gas-particle partitioning of oxidized Hg at the sampling site. Moreover, from Fig. S3B–C, a daytime-nighttime gap in T and RH of around 5 °C and 30% were observed for both the dry and rainy season. Such a temperature and RH difference could impact the Hg mass fraction, as higher T and lower RH facilitate PBM back-partitioning and likely resulted in the lower Hg mass fraction at noon in both seasons (Fig. 4C). In conclusion, both primary and secondary sources could play important roles in controlling PBM concentrations and the Hg mass fraction diurnal pattern in HCMC.

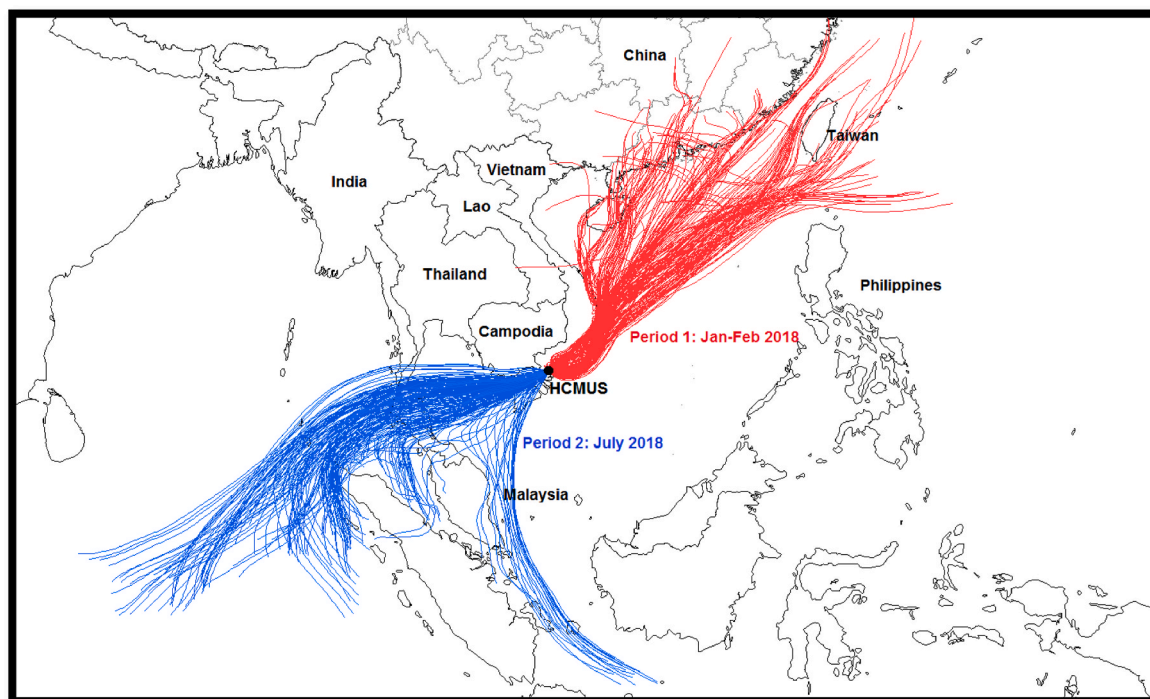


Fig. 5. 5-Day backward trajectories started from HCMUS during the dry season (period 1, red) and rainy season (period 2, blue). (For interpretation of the references to colour in this figure legend, the reader is referred to the Web version of this article.)

3.3. Source apportionment results

3.3.1. Correlation and PCA analysis

Table S1 shows the correlations among metals in PM samples collected during the study period. All metals generally show significant positive weak to moderate correlations, indicating similar origins among them (Roy et al., 2019). From Table S1, Cu showed significant correlations with all metals ($r = 0.24\text{--}0.64$, $p < 0.05$). Cu emissions often originate from heat transfer in brakes, tire corrosion or diesel combustion (Hini et al., 2020; Dat et al., 2021). Traffic activities also produce significant Pb and Cr concentrations and have been correlated with Cu (Idris et al., 2019). Moreover, a moderate Ni–Cr correlation ($r = 0.52$, $p < 0.01$) indicated inputs from electroforming, electroplating and circuitry (Hini et al., 2020), while moderate Cu–Ni ($r = 0.52$, $p < 0.01$) and Cu–As ($r = 0.64$, $p < 0.01$) correlations further suggested Cu inputs from industrial activities (Kabadayi and Cesur, 2010). Therefore, additional sources other than traffic activity also influenced Cu concentration at HCMC. Besides, As is a typical indicator for combustion activity (i.e. in power plants or heating), and coal quality (i.e. particle size, carbon content) can heavily influence As emission rates (Zhang et al., 2018; Lin et al., 2018). As a result, inter-element correlations with As are often attributed to anthropogenic activity, which was seen for most metals in our study ($r = 0.29\text{--}0.64$, $p < 0.01$). More studies are incorporating Sr as an indicator for crustal sources for airborne particulate matter in urban areas (Amil et al., 2016; Wu et al., 2019). At HCMC, positive correlations were observed between Sr–Al ($r = 0.93$, $p < 0.01$) and Sr–Mn ($r = 0.52$, $p < 0.01$) while negative correlations were observed for others. This suggests Sr, Al, and Mn originate from sources that differ from the rest of metals. Studies have demonstrated that Al and Mn are core elements in ores and minerals that often associate with crustal origins (USEPA, 2002; Idris et al., 2019). Therefore, the moderate Al–Mn correlation ($r = 0.56$, $p < 0.01$) may represent natural source contributions to PM at HCMC. On the other hand, Hg (i.e. PBM_{10}) showed significant correlations with selected metals ($p < 0.01$), in which negative correlations were seen for Al ($r = -0.23$), Sr ($r = -0.32$) and positive correlations for others ($r = 0.28\text{--}0.62$). Therefore, owing to the positive correlations, Hg

might share similar origins with most metals except for Al and Sr. Moreover, better correlations were obtained for Hg with Cu ($r = 0.62$) and As ($r = 0.59$) as compared to other metals, implying anthropogenic activities are an important Hg source in HCMC.

Source apportionment for PM composition at HCMC was investigated by employing PCA. A KMO value greater than 0.6 is required for PCA data adequacy (Jamhari et al., 2014; Dat et al., 2021), and our dataset achieved a KMO of 0.75. Three principal components (PCs) were extracted in the final solution (Table 3), in which the first PC explained 32.4% of the total variability, followed by another 23.7% and 16.3% by the second and third PCs. Strong positive PBM, As and Cu loadings (i.e. > 0.7), and moderate Cr, Pb, and Ni loadings characterized PC1, implying influences from combustion, anthropogenic and industrial activities. A previous study showed non-ferrous metal smelting and cement production as sources of street dust in HCMC (Dat et al., 2021), which could also act as PM_{10} sources and support our attribution for sources related to PC1. PC2 was characterized by strong Al, Mn, and Sr loadings, indicating influences from natural sources (Amil et al., 2016; Wu et al., 2019). High abundances of mineral elements (e.g. Fe, Al, Mn) could be either of mineral or crustal origin, possibly from road expansion and building construction in metropolitan areas (Tripathee et al., 2014; Liu et al., 2019; Guo et al., 2020; Dat et al., 2021). In PC3, a strong positive RH loading and a strong temperature negative loading represented impacts of meteorological factors on ambient PM in HCMC. These parameters are also intertwined with aerosol secondary formation processes, with an emphasis on Hg gas-particle partitioning.

From Table 3, it can be seen that PBM only has a significant loading in PC1 and PC3, with a value 3 times higher in PC1 (0.75) than in PC3 (0.24). Therefore, anthropogenic and industrial activities were identified as primary PBM sources in HCMC, notably from combustion, traffic and industrial activities. Besides, meteorological parameters represent contribution from secondary formation processes to PBM variation, but to a lesser extent. A near-zero PBM loading was found in PC2, implying a minimal contribution from natural sources to the PBM variation. Our finding slightly differs from sites in Kathmandu Valley, Nepal (Guo et al., 2017, 2020, 2021) where influences of crustal sources on PBM

Table 3
Varimax rotated factor loadings for the PM₁₀ dataset in Ho Chi Minh City.

PC	Sources or processes being identified with	Hg	Al	Mn	Cu	Cr	Pb	Ni	As	Sr	RH	Temp	Eigen-values	% Variance
1	Combustion, traffic and industrial activities	0.75	-0.23	0.55	0.83	0.75	0.37	0.66	0.79	-0.31	-0.26	-0.19	3.6	32.4
2	Natural sources	-0.09	0.94	0.77	-0.31	0.17	0.03	-0.19	-0.14	0.92	0.21	0.20	2.6	23.7
3	Secondary formation	0.24	0.07	-0.15	-0.10	-0.27	0.28	-0.20	0.17	0.01	0.85	-0.86	1.8	16.3

concentration was observed, but agreed with sites in China (Liu et al., 2019; Qin et al., 2019) where high Hg emission intensity controlled PBM concentrations. From the PCA results, contributions of both primary and secondary sources are highlighted and reinforce our findings in previous sections. However, PCA remains our preliminary step to acquire information of PBM₁₀ sources in HCMC. Other tools including Hg isotope analysis might be a promising tool to fully understand the PBM sources and their transformation, which could be a topic of an upcoming study.

3.3.2. Cluster analysis

From Fig. S6, four main clusters were classified from air masses reaching HCMC in two seasons, and their corresponding PBM and PM concentrations were determined (Table S2). The lowest PM concentrations were observed in cluster 3, at $98.7 \mu\text{g m}^{-3}$ and $30.3 \mu\text{g m}^{-3}$ for the dry and rainy season, respectively. These clusters spent most of their time over the ocean, thus could be classified as clean air masses with low PM concentration (Zheng et al., 2021b; Jiang et al., 2021). For PBM concentrations, however, a relatively higher level was observed in the dry season for cluster 3 (81.4pg m^{-3}) as compared to others. This could be explained by PBM enrichment by halogen radicals through oxidized Hg accumulation on aqueous super-micron sea salt aerosols within the MBL (Mason and Sheu, 2002; Ariya et al., 2015; Mao et al., 2016).

In contrast, clusters 1, 2 and 4 in both seasons exhibited similar transport pathways, passing continental regions with higher Hg emission density, which could lead to higher PM concentrations. However, as a higher ambient temperature was observed for cluster 2 (30.4°C) than other clusters ($26.2\text{--}28.3^\circ\text{C}$) in the dry season, a greater back-partitioning process might lead to the lower PBM concentration. Nonetheless, owing to an abundance of local sources at HCMC, only slight differences in PM ($\sim 20\%$) and PBM ($\sim 15\%$) concentrations were observed between marine and continental clusters. Therefore, although the air mass transport path might partially govern PM and/or PBM concentrations, the stronger impact from local sources disrupted its influence resulting in an unclear pattern among different clusters.

3.4. Health effects assessment

In this study, we evaluated the non-carcinogenic health risk for children and adults living in HCMC. For adults, HQ values decrease in the order of ingestion (7.3×10^{-3}) > dermal contact (2.2×10^{-5}) > inhalation (3.3×10^{-6}), with a total HI index of 7.6×10^{-4} . A similar sequence was also found for children, with HQ indices of 8.1×10^{-3} , 1.7×10^{-4} , and 6.8×10^{-6} respectively. With an 11-time higher HI index, children are a more vulnerable target of PBM long-term exposure than adults. However, these values are all lower than the safe level (HI < 1) which suggests a tolerable level of PBM non-carcinogenic risk to HCMC residents. Since a dry > rainy pattern was observed for PBM concentration, higher pollutant levels in dry months can impact public health more seriously, especially with projected industrial expansion in the near future.

Ingestion is the major pathway of PBM exposure in HCMC, which is consistent with similar studies in China (Huang et al., 2014; Wang et al., 2014). Exposure by ingestion is more common among children since they involuntarily ingest or inhale greater PM amounts, thus might consume more PBM (Moya et al., 2004; Pan et al., 2016). Besides, finer particles may contain a higher Hg mass fraction which could re-suspend

in the atmosphere and enter the respiratory system (Lu et al., 2014). Therefore, inhalation HQ index could be underestimated without additional contributions from other size fractions. On the other hand, since Hg can get absorbed via the epidermis and intrusion via sweat glands and hair follicles (Park and Zheng, 2012), PBM dermal exposure may be serious in tropical metropolitan cities where residents wear more lightweight clothing in comparison with mid-latitude regions (Schleicher et al., 2016; Fang et al., 2018). Furthermore, as atmospheric PBM only constitutes a minor proportion, evaluation of other Hg species (i.e. GEM and GOM) is also essential to consider the atmospheric Hg health risk to a fuller extent (Pyta et al., 2020). To date, PBM health risk evaluation has been primarily conducted for street dust (Moreda-Piñeiro et al., 2020; Cui et al., 2020) while similar studies for ambient particulate matter remain scarce. The results collected in this study lay a good foundation to further access Hg in various media and complement Hg understanding on a regional level. Also, speculation of GEM and GOM levels in HCMC is crucial as Hg gas-partitioning is considered a governing mechanism for atmospheric Hg in this area.

4. Conclusions

In this study, two intensive sampling campaigns were conducted to characterize PBM₁₀ and the Hg mass fraction at a megacity in Southeast Asia. In 2018, average PBM concentrations and Hg mass fraction were $67.3 \pm 45.9 \text{pg m}^{-3}$ and $1.18 \pm 1.12 \mu\text{g g}^{-1}$. Although moderate PBM concentrations were observed as compared to other polluted megacities, a comparable Hg mass fraction to that in metropolitan areas in China was observed, highlighting the influence of anthropogenic sources on PBM accumulation in HCMC. Furthermore, significant positive PBM–PM and PBM–PBM/PM correlations ($R^2 = 0.11\text{--}0.52$, $p < 0.01$) indicated similar primary and secondary sources govern the PBM and PM variations. For seasonal trends, a dry > rainy pattern was observed for PBM concentrations owing to greater wet scavenging and dry deposition in the rainy season. Anthropogenic emissions and gas-particle partitioning of oxidized Hg were predominant factors governing PBM and Hg mass fraction diurnal patterns at HCMC. PCA revealed that PBM sources were mainly attributed to anthropogenic emissions (i.e. combustion, traffic, and industrial origins) and a possible contribution from gas-particle partitioning. A health risk evaluation portrayed minimal PBM exposure for children and adults in HCMC with non-carcinogenic effects (HI < 1), but extra precautions should be taken for dermal exposure among local residents. Further evaluations using Hg information from other media as well as GEM/GOM concentrations would complement the data presented here as well as improve Hg regional understanding. This study helps fill the data gap on Hg pollution worldwide while laying the groundwork to establish local regulations and motivating upcoming Hg studies within the region.

Credit of authors statement

Ly Sy Phu Nguyen: Resources, Conceptualization, Methodology, Investigation, Supervision, Writing-original draft, Writing-review & editing. **To Thi Hien:** Resources, Writing-review & editing. **Minh Tri Truong:** Methodology, Investigation, Conceptualization, Writing-review & editing. **Nguyen Doan Thien Chi:** Visualization, Investigation. **Guey-Rong Sheu:** Resources, Visualization, Supervision, Writing -

review & editing.

Declaration of competing interest

The authors declare that they have no known competing financial interests or personal relationships that could have appeared to influence the work reported in this paper.

Data availability

Data will be made available on request.

Acknowledgements

We gratefully thank the members of the Air and water pollution - Public Health - Climate Change research group of Faculty of Environment, VNUHCM-University of Science for instrument operation and maintenance at the observation site. This research is funded by Vietnam National University, Ho Chi Minh City (VNU-HCM) under grant number C2022-18-33.

Appendix A. Supplementary data

Supplementary data to this article can be found online at <https://doi.org/10.1016/j.chemosphere.2022.135707>.

References

- Amil, N., Latif, M.T., Khan, M.F., Mohamad, M., 2016. Seasonal variability of PM_{2.5} composition and sources in the Klang Valley urban-industrial environment. *Atmos. Chem. Phys.* 16 (8), 5357–5381.
- Amos, H.M., Jacob, D.J., Holmes, C.D., Fisher, J.A., Wang, Q., Yantosca, R.M., Corbett, E. S., Galarneau, E., Rutter, A.P., Gustin, M.S., Steffen, A., Schauer, J.J., Graydon, J.A., Louis, V.L.S., Talbot, R.W., Edgerton, E.S., Zhang, Y., Sunderland, E.M., 2012. Gas-particle partitioning of atmospheric Hg(II) and its effect on global mercury deposition. *Atmos. Chem. Phys.* 12, 591–603.
- Andreoli, V., Sprovieri, F., 2017. Genetic aspects of susceptibility to mercury toxicity: an overview. *Int. J. Environ. Res. Public Health* 14, 93.
- Ariya, P.A., Amyot, M., Dastoor, A., Deeds, D., Feinberg, A., Kos, G., Poulain, A., Ryjkov, A., Semeniuk, K., Subir, M., 2015. Mercury physicochemical and biogeochemical transformation in the atmosphere and at atmospheric interfaces: a review and future directions. *Chem. Rev.* 115, 3760–3802.
- Beckers, F., Rinklebe, J., 2017. Cycling of mercury in the environment: sources, fate, and human health implications: a review. *Crit. Rev. Environ. Sci. Technol.* 47 (9), 693–794.
- Buchard, V., Randles, C.A., Da Silva, A.M., Darmenov, A., Colarco, P.R., Govindaraju, R., Ferrare, R., Hair, J., Beyersdorf, A.J., Ziemba, L.D., Yu, H., 2017. The MERRA-2 aerosol reanalysis, 1980 onward. Part II: evaluation and case studies. *J. Clim.* 30, 6851–6872.
- Chand, D., Jaffe, D., Prestbo, E., Swartzendruber, P.C., Hafner, W., Weiss-Penzias, P., Kato, S., Takami, A., Hatakeyama, S., Kajii, Y., 2008. Reactive and particulate mercury in the Asian marine boundary layer. *Atmos. Environ.* 42 (34), 7988–7996.
- Chen, X., Balasubramanian, R., Zhu, Q., Behera, S.N., Bo, D., Huang, X., Xie, H., Cheng, J., 2016. Characteristics of atmospheric particulate mercury in size-fractionated particles during haze days in Shanghai. *Atmos. Environ.* 131, 400–408.
- Cheng, L., Zhang, L., Blanchard, P., 2014. Regression modeling of gas-particle partitioning of atmospheric oxidized mercury from temperature data. *J. Geophys. Res.* 119, 11864–11876.
- Choi, H.D., Huang, J., Mondal, S., Holsen, T.M., 2013. Variation in concentrations of three mercury (Hg) forms at a rural and a suburban site in New York State. *Sci. Total Environ.* 448, 96–106.
- Cui, L., Wu, Z., Han, P., Taira, Y., Wang, H., Meng, Q., Feng, Z., Zhai, S., Yu, J., Zhu, W., Kong, Y., 2020. Chemical content and source apportionment of 36 heavy metal analysis and health risk assessment in aerosol of Beijing. *Environ. Sci. Pollut. Res.* 27 (7), 7005–7014.
- Dat, N.D., Nguyen, V.-T., Bui, X.-T., Bui, M.-H., Nguyen, L.S.P., Nguyen, X.-C., Tran, A.T.-K., Ju, Y.-R., Nguyen, D.-H., Bui, H.-N., 2021. Contamination, source attribution, and potential health risks of heavy metals in street dust of a metropolitan area in Southern Vietnam. *Environ. Sci. Pollut. Res.* 1–15.
- De Simone, F., Artaxo, P., Bencardino, M., Cinnirella, S., Carbone, F., D'Amore, F., Dommergue, A., Feng, X.B., Gencarelli, C.N., Hedgecock, I.M., Landis, M.S., Sprovieri, F., Suzuki, N., Wängberg, I., Pirrone, N., 2017. Particulate-phase mercury emissions from biomass burning and impact on resulting deposition: a modelling assessment. *Atmos. Chem. Phys.* 17, 1881–1899.
- Draxler, R.R., Rolph, G.D., 2010. HYSPLIT (HYbrid Single-Particle Lagrangian Integrated Trajectory) Model Access via NOAA ARL READY Website. NOAA Air Resources Laboratory. Silver Spring, MD, p. 25 <http://ready.arl.noaa.gov/HYSPLIT.php>.
- Driscoll, C.T., Mason, R.P., Chan, H.M., Jacob, D.J., Pirrone, N., 2013. Mercury as a global pollutant: sources, pathways, and effects. *Environ. Sci. Technol.* 47, 4967–4983.
- Fang, G.C., Chen, Y.C., Lo, C.T., Cho, M.H., Zhuang, Y.J., Tsai, K.H., Huang, C.Y., Xiao, Y. F., 2018. Concentrations and analysis of health risks of ambient air metallic elements at Longjing site in central Taiwan. *Environ. Geochem. Health* 40 (1), 461–472.
- Fu, X.W., Zhang, H., Yu, B., Wang, X., Lin, C.J., Feng, X.B., 2015. Observations of atmospheric mercury in China: a critical review. *Atmos. Chem. Phys.* 15, 9455–9476.
- Fu, X., Yang, X., Lang, X., Zhou, J., Zhang, H., Yu, B., Yan, H., Lin, C.-J., Feng, X., 2016. Atmospheric wet and litterfall mercury deposition at urban and rural sites in China. *Atmos. Chem. Phys.* 16, 11547–11562.
- Gratz, L.E., Keeler, G.J., Marsik, F.J., Barres, J.A., Dvonch, J.T., 2013. Atmospheric transport of speciated mercury across southern Lake Michigan: influence from emission sources in the Chicago/Gary urban area. *Sci. Total Environ.* 448, 84–95.
- Guo, J., Kang, S., Huang, J., Zhang, Q., Rupakheti, M., Sun, S., Tripathee, L., Rupakheti, D., Panday, A.K., Sillanpää, M., 2017. Characterizations of atmospheric particulate-bound mercury in the Kathmandu Valley of Nepal, south Asia. *Sci. Total Environ.* 579, 1240–1248.
- Guo, J., Ram, K., Tripathee, L., Kang, S., Huang, J., Chen, P., Ghimire, P.S., 2020. Study on mercury in PM₁₀ at an urban site in the central indo-gangetic plain: seasonal variability and influencing factors. *Aerosol Air Qual. Res.* 20, 2729–2740.
- Guo, J., Sharma, C.M., Tripathee, L., Kang, S., Fu, X., Huang, J., Shrestha, K.L., Chen, P., 2021. Source identification of atmospheric particle-bound mercury in the Himalayan foothills through non-isotopic and isotope analyses. *Environ. Pollut.* 286, 117317.
- Han, D., Zhang, J., Hu, Z., Ma, Y., Duan, Y., Han, Y., Chen, X., Zhou, Y., Cheng, J., Wang, W., 2018. Particulate mercury in ambient air in Shanghai, China: size-specific distribution, gas-particle partitioning, and association with carbonaceous composition. *Environ. Pollut.* 238, 543–553.
- Hien, D.T., Khai, N.M., Van Ton, D., Binh, V.T.C., Lan, N.T., 2018. An initial analysis and evaluation of mercury content in raw coal samples used in some coal-fired thermal power plants in Vietnam. *VNU J. Sci.: Earth and Environ. Sci.* 34 (4).
- Hien, T.T., Chi, N.D.T., Nguyen, N.T., Takenaka, N., Huy, D.H., 2019. Current status of fine particulate matter (PM_{2.5}) in Vietnam's most populous city, Ho Chi Minh City. *Aerosol Air Qual. Res.* 19, 2239–2251.
- Hini, G., Eziz, M., Wang, W., Ili, A., Li, X., 2020. Spatial distribution, contamination levels, sources, and potential health risk assessment of trace elements in street dusts of Urumqi city, NW China. *Hum. Ecol. Risk Assess.* 26, 2112–2128.
- Huang, M., Chen, X., Shao, D., Zhao, Y., Wang, W., Wong, M.H., 2014. Risk assessment of arsenic and other metals via atmospheric particles, and effects of atmospheric exposure and other demographic factors on their accumulations in human scalp hair in urban area of Guangzhou, China. *Ecotoxicol. Environ. Saf.* 102, 84–92.
- Huang, J., Kang, S., Guo, J., Zhang, Q., Cong, Z., Sillanpää, M., Zhang, G., Sun, S., Tripathee, L., 2016. Atmospheric particulate mercury in Lhasa city, Tibetan Plateau. *Atmos. Environ.* 142, 433–441.
- Huang, Q., Reinfelder, J.R., Fu, P., Huang, W., 2020. Variation in the mercury concentration and stable isotope composition of atmospheric total suspended particles in Beijing, China. *J. Hazard Mater.* 383, 121131.
- Idris, A.M., Alqahtani, F.M.S., Said, T.O., Fawy, K.F., 2019. Contamination level and risk assessment of heavy metal deposited in street dusts in Khamees-Mushait city, Saudi Arabia. *Hum. Ecol. Risk Assess.* 26, 495–511.
- Illuminati, S., Annibaldi, A., Bau, S., Scarchilli, C., Ciardini, V., Grigioni, P., Girolametti, F., Vagnoni, F., Scarponi, G., Truzzi, C., 2020. Seasonal evolution of size-segregated particulate mercury in the atmospheric aerosol over Terra Nova Bay, Antarctica. *Molecules* 25 (17), 3971.
- Jamhari, A.A., Sahani, M., Latif, M.T., Chan, K.M., Tan, H.S., Khan, M.F., Tahir, N.M., 2014. Concentration and source identification of polycyclic aromatic hydrocarbons (PAHs) in PM₁₀ of urban, industrial and semi-urban areas in Malaysia. *Atmos. Environ.* 86, 16–27.
- Jiang, B., Xie, Z., Lam, P.K., He, P., Yue, F., Wang, L., Huang, Y., Kang, H., Yu, X., Wu, X., 2021. Spatial and temporal distribution of sea salt aerosol mass concentrations in the marine boundary layer from the Arctic to the Antarctic. *J. Geophys. Res.* 126 (6), e33892.
- Kabadayi, F., Cesur, H., 2010. Determination of Cu, Pb, Zn, Ni, Co, Cd, and Mn in road dusts of Samsun City. *Environ. Monit. Assess.* 168 (1), 241–253.
- Keeler, G., Glinson, G., Pirrone, N., 1995. Particulate mercury in the atmosphere: its significance, transport, transformation and sources. *Wat. Air and Soil Poll.* 80 (1), 159–168.
- Kim, P.R., Han, Y.J., Holsen, T.M., Yi, S.M., 2012. Atmospheric particulate mercury: concentrations and size distributions. *Atmos. Environ.* 61, 94–102.
- Le, P.V., Phan-Van, T., Mai, K.V., Tran, D.Q., 2019. Space-time variability of drought over Vietnam. *Int. J. Climatol.* 39, 5437–5451.
- Lin, Y.C., Hsu, S.C., Lin, C.Y., Lin, S.H., Huang, Y.T., Chang, Y., Zhang, Y.L., 2018. Enhancements of airborne particulate arsenic over the subtropical free troposphere: impact of southern Asian biomass burning. *Atmos. Chem. Phys.* 18, 13865–13879.
- Liu, J., Wang, L., Zhu, Y., Lin, C.-J., Jang, C., Wang, S., Xing, J., Yu, B., Xu, H., Pan, Y., 2019. Source attribution for mercury deposition with an updated atmospheric mercury emission inventory in the Pearl River Delta Region, China. *Front. Environ. Sci. Eng.* 13, 2.
- Lu, X., Wu, X., Wang, Y., Chen, H., Gao, P., Fu, Y., 2014. Risk assessment of toxic metals in street dust from a medium-sized industrial city of China. *Ecotoxicol. Environ. Saf.* 106, 154–163.
- Mao, H., Talbot, R., Hegarty, J., Koerner, J., 2012. Speciated mercury at marine, coastal, and inland sites in New England-Part 2: relationships with atmospheric physical parameters. *Atmos. Chem. Phys.* 12 (9), 4181–4206.

- Mao, H., Cheng, I., Zhang, L., 2016. Current understanding of the driving mechanisms for spatiotemporal variations of atmospheric speciated mercury: a review. *Atmos. Chem. Phys.* 16, 12897–12924.
- Mason, R.P., Sheu, G.-R., 2002. Role of the ocean in the global mercury cycle. *Global Biogeochem. Cycles* 16, 1093.
- McLagan, D.S., Mazur, M.E., Mitchell, C.P., Wania, F., 2016. Passive air sampling of gaseous elemental mercury: a critical review. *Atmos. Chem. Phys.* 16 (5), 3061–3076.
- McLagan, D.S., Monaci, F., Huang, H., Lei, Y.D., Mitchell, C.P., Wania, F., 2019. Characterization and quantification of atmospheric mercury sources using passive air samplers. *J. Geophys. Res. Atmos.* 124 (4), 2351–2362.
- Moreda-Piñeiro, J., Rodríguez-Cabo, A., Fernández-Amado, M., Piñeiro-Iglesias, M., Muniategui-Lorenzo, S., López-Mahía, P., 2020. Levels and sources of atmospheric particle-bound mercury in atmospheric particulate matter (PM10) at several sites of an Atlantic Coastal European Region. *Atmosphere* 11 (1), 33.
- Moya, J., Bearer, C.F., Etzel, R.A., 2004. Children's behavior and physiology and how it affects exposure to environmental contaminants. *Pediatrics* 113, 996–1006.
- Nguyen, L.S.P., Sheu, G.-R., 2019. Four-year measurements of wet mercury deposition at a tropical mountain site in central Taiwan. *Aerosol Air Qual. Res.* 19, 2043–2055.
- Nguyen, L.S.P., Sheu, G.-R., Lin, D.-W., Lin, N.-H., 2019a. Temporal changes in atmospheric mercury concentrations at a background mountain site downwind of the East Asia continent in 2006–2016. *Sci. Total Environ.* 686, 1049–1056.
- Nguyen, L.S.P., Zhang, L., Lin, D.-W., Lin, N.-H., Sheu, G.-R., 2019b. Eight-year dry deposition of atmospheric mercury to a tropical high mountain background site downwind of the East Asian continent. *Environ. Pollut.* 225, 113128.
- Nguyen, L.S.P., Sheu, G.-R., Chang, S.C., Lin, N.H., 2021a. Effects of temperature and relative humidity on the partitioning of atmospheric oxidized mercury at a high-altitude mountain background site in Taiwan. *Atmos. Environ.* 261, 118572.
- Nguyen, L.S.P., Sheu, G.-R., Hsiao, T.-C., Lee, C.-T., Chang, S.-C., Lin, N.-H., 2021b. Relationships between atmospheric mercury and optical properties of spring outflow aerosols from Southeast Asia. *Atmos. Pollut. Res.* 12, 101178.
- Nguyen, L.S.P., Nguyen, K.T., Griffith, S.M., Sheu, G.R., Yen, M.C., Chang, S.C., Lin, N.H., 2022a. Multiscale temporal variations of atmospheric mercury distinguished by the Hilbert – Huang transform analysis reveals multiple El Niño–Southern oscillation links. *Environ. Sci. Technol.* 56, 1423–1432.
- Nguyen, L.S.P., Chang, J.H.W., Griffith, S.M., Hien, T.T., Kong, S.S.K., Le, H.N., Huang, H.Y., Sheu, G.-R., Lin, N.H., 2022b. Trans-boundary air pollution in a Southeast Asian megacity: case studies of the synoptic meteorological mechanisms and impacts on air quality. *Atmos. Pollut. Res.* 13, 101366.
- Obrist, D., Kirk, J.L., Zhang, L., Sunderland, E.M., Jiskra, M., Selin, N.E., 2018. A review of global environmental mercury processes in response to human and natural perturbations: changes of emissions, climate, and land use. *Ambio* 47, 116–140.
- Pan, L., Ma, J., Hu, Y., Su, B., Fang, G., Wang, Y., Wang, Z., Wang, L., Xiang, B., 2016. Assessments of levels, potential ecological risk, and human health risk of heavy metals in the soils from a typical county in Shanxi Province, China. *Environ. Sci. Pollut. Res.* 23 (19), 19330–19340.
- Park, J.D., Zheng, W., 2012. Human exposure and health effects of inorganic and elemental mercury. *J. Prev. Med. Publ. Health* 45 (6), 344.
- Phung, D., Hien, T.T., Linh, H.N., Luong, L.M., Morawska, L., Chu, C., Binh, N.D., Thai, P. K., 2016. Air pollution and risk of respiratory and cardiovascular hospitalizations in the most populous city in Vietnam. *Sci. Total Environ.* 557, 322–330.
- Poissant, L., Pilote, M., Beauvais, C., Constant, P., Zhang, H.H., 2005. A year of continuous measurements of three atmospheric mercury species (GEM, RGM and Hg_p) in southern Quebec, Canada. *Atmos. Environ.* 39 (7), 1275–1287.
- Pyta, H., Rogula-Kozłowska, W., 2016. Determination of mercury in size-segregated ambient particulate matter using CVAAS. *Microchem. J.* 124, 76–81.
- Pyta, H., Widziejewicz-Rzońca, K., Slaby, K., 2020. Inhalation exposure to gaseous and particulate bound mercury present in the ambient air over the polluted area of southern Poland. *Int. J. Environ. Res. Public Health* 17 (14), 4999.
- Qin, X., Wang, X., Shi, Y., Yu, G., Zhao, N., Lin, Y., Fu, Q., Wang, D., Xie, Z., Deng, C., Huang, K., 2019. Characteristics of atmospheric mercury in a suburban area of east China: sources, formation mechanisms, and regional transport. *Atmos. Chem. Phys.* 19 (9), 5923–5940.
- Ren, X., Luke, W.T., Kelley, P., Cohen, M.D., Artz, R., Olson, M.L., Schmeltz, D., Puchalski, M., Goldberg, D.L., Ring, A., Mazzuca, G.M., Cummings, K.A., Wojdan, L., Preaux, S., Stehr, J.W., 2016. Atmospheric mercury measurements at a suburban site in the Mid-Atlantic United States: inter-annual, seasonal and diurnal variations and source-receptor relationships. *Atmos. Environ.* 146, 141–152.
- Roy, S., Gupta, S.K., Prakash, J., Habib, G., Baudh, K., Nasr, M., 2019. Ecological and human health risk assessment of heavy metal contamination in road dust in the National Capital Territory (NCT) of Delhi, India. *Environ. Sci. Pollut. Res.* 26 (29), 30413–30425.
- Rutter, A.P., Schauer, J.J., 2007. The effect of temperature on the gas–particle partitioning of reactive mercury in atmospheric aerosols. *Atmos. Environ.* 41, 8647–8657.
- Sakata, M., Marumoto, K., 2002. Formation of atmospheric particulate mercury in the Tokyo metropolitan area. *Atmos. Environ.* 36 (2), 239–246.
- Schleicher, N., Schäfer, J., Chen, Y., Blanc, G., Chai, F., Cen, K., Norra, S., 2016. Atmospheric particulate mercury in the megacity Beijing: efficiency of mitigation measures and assessment of health effects. *Atmos. Environ.* 124, 396–403.
- Sheu, G.-R., Lin, N.-H., Wang, J.-L., Lee, C.-T., Yang, C.-F.O., Wang, S.-H., 2010. Temporal distribution and potential sources of atmospheric mercury measured at a high-elevation background station in Taiwan. *Atmos. Environ.* 44, 2393–2400.
- Sheu, G.-R., Lin, N.-H., 2013. Characterizations of wet mercury deposition to a remote islet (Pengjiayu) in the subtropical Northwest Pacific Ocean. *Atmos. Environ.* 77, 474–481.
- Sheu, G.-R., Nguyen, L.S.P., Truong, M.T., Lin, D.-W., 2019. Characteristics of atmospheric mercury at a suburban site in northern Taiwan and influence of trans-boundary haze events. *Atmos. Environ.* 214, 116827.
- Siudek, P., Frankowski, M., Siepak, J., 2016. Atmospheric particulate mercury at the urban and forest sites in central Poland. *Environ. Sci. Pollut. Res.* 23 (3), 2341–2352.
- Soerensen, A.L., Skov, H., Jacob, D.J., Soerensen, B.T., Johnson, M.S., 2010. Global concentrations of gaseous elemental mercury and reactive gaseous mercury in the marine boundary layer. *Environ. Sci. Technol.* 44 (19), 7425–7430.
- Song, X., Cheng, I., Lu, J., 2009. Annual atmospheric mercury species in downtown Toronto, Canada. *Environ. Monit. Assess.* 11 (3), 660–669.
- Sproveri, F., Hedgecock, I.M., Pirrone, N., 2010. An investigation of the origins of reactive gaseous mercury in the Mediterranean marine boundary layer. *Atmos. Chem. Phys.* 10 (8), 3985–3997.
- Steffen, A., Bottenheim, J., Cole, A., Douglas, T.A., Ebinghaus, R., Friess, U., Netcheva, S., Nghiem, S., Sihler, H., Staebler, R., 2013. Atmospheric mercury over sea ice during the OASIS-2009 campaign. *Atmos. Chem. Phys.* 13 (14), 7007–7021.
- Tang, Y., Wang, S., Wu, Q., Liu, K., Li, Z., Zou, J., Hou, D., Wu, Y., Duan, L., 2019. Measurement of size-fractionated particulate-bound mercury in Beijing and implications on sources and dry deposition of mercury. *Sci. Total Environ.* 675, 176–183.
- Tripathee, L., Kang, S., Huang, J., Sharma, C.M., Sillanpää, M., Guo, J., Paudyal, R., 2014. Concentrations of trace elements in wet deposition over the central Himalayas, Nepal. *Atmos. Environ.* 95, 231–238.
- Truong, M.T., Nguyen, L.S.P., Hien, T.T., Pham, T.D.H., Do, T.T.L., 2022. Source apportionment and risk estimation of heavy metals in PM₁₀ at a southern Vietnam megacity. *Aerosol Air Qual. Res.* 22, 220094.
- UN Environment, 2019. Global Mercury Assessment 2018. UN Environment Programme. Chemicals and Health Branch Geneva, Switzerland.
- UNEP, 2013. UNEP: Global Mercury Assessment 2013: Sources, Emissions, Releases and Environmental Transport. UNEP Chemicals Branch, Geneva, Switzerland.
- USEPA, 2002. Supplemental Guidance for Developing Soil Screening Levels for Superfund Sites. Environmental Protection Agency, Washington, DC.
- Wang, Y.Q., Zhang, X.Y., Draxler, R.R., 2009. TrajStat: GIS-based software that uses various trajectory statistical analysis methods to identify potential sources from long-term air pollution measurement data. *Environ. Model. Software* 24, 938–939.
- USEPA, 2017. Update for chapter 5 of the exposure factors handbook. In: Soil and Dust Ingestion. Environmental Protection Agency. EPA/600/R-17/384F, Washington, DC.
- Wang, L., Lu, X., Ren, C., Li, X., Chen, C., 2014. Contamination assessment and health risk of heavy metals in dust from Changqing industrial park of Baoji, NW China. *Environ. Earth Sci.* 71, 2095–2104.
- Weiss-Penzias, P., Amos, H.M., Selin, N.E., Gustin, M.S., Jaffe, D.A., Obrist, D., Sheu, G. R., Giang, A., 2015. Use of a global model to understand speciated atmospheric mercury observations at five high-elevation sites. *Atmos. Chem. Phys.* 15 (3), 1161–1173.
- WHO, 2000. Air quality guidelines for Europe. *Eur. Ser.* 3 (1), 23.
- Wu, Q., Wang, S., Li, G., Liang, S., Lin, C.-J., Wang, Y., Cai, S., Liu, K., Hao, J., 2016. Temporal trend and spatial distribution of speciated atmospheric mercury emissions in China during 1978–2014. *Environ. Sci. Technol.* 50, 13428–13435.
- Wu, Q., Gao, W., Wang, S., Hao, J., 2017. Updated atmospheric speciated mercury emissions from iron and steel production in China during 2000–2015. *Atmos. Chem. Phys.* 17, 10423–10433.
- Wu, R., 2017. Relationship between Indian and East Asian summer rainfall variations. *Adv. Atmos. Sci.* 34 (1), 4–15.
- Wu, L., Luo, X.S., Li, H., Cang, L., Yang, J., Zhao, Z., Tang, M., 2019. Seasonal levels, sources, and health risks of heavy metals in atmospheric PM_{2.5} from four functional areas of Nanjing city, eastern China. *Atmosphere* 10 (7), 419.
- Xiu, G.L., Jin, Q., Zhang, D., Shi, S., Huang, X., Zhang, W., Bao, L., Gao, P., Chen, B., 2005. Characterization of size-fractionated particulate mercury in Shanghai ambient air. *Atmos. Environ.* 39 (3), 419–427.
- Xu, L., Chen, J., Yang, L., Niu, Z., Tong, L., Yin, L., Chen, Y., 2015. In: Characteristics and Sources of Atmospheric Mercury Speciation in a Coastal City, Xiamen, China. *Chemosphere*, 119, 530–539.
- Yu, G., Qin, X., Xu, J., Zhou, Q., Wang, B., Huang, K., Deng, C., 2019. Characteristics of particulate-bound mercury at typical sites situated on dust transport paths in China. *Sci. Total Environ.* 648, 1151–1160.
- Zhang, H., Fu, X., Wang, X., Feng, X., 2019. Measurements and distribution of atmospheric particulate-bound mercury: a review. *Bull. Environ. Contam. Toxicol.* 103 (1), 48–54.
- Zhang, L., Wang, S.X., Wang, L., Wu, Y., Duan, L., Wu, Q.R., Wang, F.Y., Yang, M., Yang, H., Hao, J.M., Liu, X., 2015a. Updated emission inventories for speciated atmospheric mercury from anthropogenic sources in China. *Environ. Sci. Technol.* 49, 3185–3194.
- Zhang, Y., Liu, R., Wang, Y., Cui, X., Qi, J., 2015b. Change characteristic of atmospheric particulate mercury during dust weather of spring in Qingdao, China. *Atmos. Environ.* 102, 376–383.
- Zhang, W., Sun, Q., Yang, X., 2018. Thermal effects on arsenic emissions during coal combustion process. *Sci. Total Environ.* 612, 582–589.
- Zheng, J., Li, M., Tang, B., Luo, W., Ma, Y., Ren, M., Yu, Y., Luo, X., Mai, B., 2021a. Levels, spatial distribution, and impact factors of heavy metals in the hair of

- metropolitan residents in China and human health implications. *Environ. Sci. Technol.* 55 (15), 10578–10588.
- Zheng, G., Wang, Y., Wood, R., Jensen, M.P., Kuang, C., McCoy, I.L., Matthews, A., Mei, F., Tomlinson, J.M., Shilling, J.E., Zawadowicz, M.A., 2021b. New particle formation in the remote marine boundary layer. *Nat. Commun.* 12 (1), 1–10.
- Zhu, J., Wang, T., Talbot, R., Mao, H., Yang, X., Fu, C., Sun, J., Zhuang, B., Li, S., Han, Y., 2014. Characteristics of atmospheric mercury deposition and size-fractionated particulate mercury in urban Nanjing, China. *Atmos. Chem. Phys.* 14, 2233–2244.